Atomic Fermi gas in the unitary limit by quantum Monte Carlo methods: Effects of the interaction range

Xin Li, Jindřich Kolorenč, and Lubos Mitas

Atomic Fermi gas in the unitary limit by quantum Monte Carlo methods: Effects of the interaction range

Xin Li,[1] Jindřich Kolorenč,[1,2] and Lubos Mitas[1]

[1]*Department of Physics, North Carolina State University, Raleigh, NC 27695, USA*
[2] *I. Institut für Theoretische Physik, Universität Hamburg, Jungiusstraße 9, 20355 Hamburg, Germany*

We calculate the ground-state properties of unpolarized two-component Fermi gas with the aid of the diffusion quantum Monte Carlo (DMC) methods. Using an extrapolation to the zero effective range of the attractive two-particle interaction, we find E/E_{free} in the unitary limit to be 0.212(2), 0.407(2), 0.409(3) and 0.398(3) for 4, 14, 38 and 66 atoms, respectively. Our calculations indicate that the dependence of the total energy on the effective range of the interaction R_{eff} is sizable and the extrapolation to $R_{\mathrm{eff}} = 0$ is therefore important for reaching the true unitary limit. To test the quality of nodal surfaces and to estimate the impact of the fixed-node approximation we perform released-node DMC calculations for 4 and 14 atoms. Analysis of the released-node and the fixed-node results suggests that the main sources of the fixed-node errors are long-range correlations which are difficult to sample in the released-node approaches due to the fast growth of the bosonic noise. Besides energies, we evaluate the two-body density matrix and the condensate fraction. We find that the condensate fraction for the 66 atom system converges to 0.56(1) after the extrapolation to the zero interaction range.

I. INTRODUCTION

In recent years, the homogeneous Fermi gas with attractive interactions has been studied extensively both theoretically and experimentally due to the success in cooling atoms into ultracold dilute condensates [1–3]. By tuning the interaction strength through the Feshbach resonance [4–7], the system can cross from the Bardeen-Cooper-Schrieffer (BCS) superfluid phase, where the s-wave scattering length a_s is negative, to the Bose-Einstein condensate (BEC), where a_s is positive. Since there is no symmetry change of the quantum state involved, the system exhibits the well-known BCS-BEC crossover.

The gas is characterized by three length parameters: the scattering length a_s, the mean interparticle spacing r_s and the effective range of the two-particle potential R_{eff}. In the special case corresponding to the diverging scattering length, $a_s \to \infty$, and to a high degree of dilution, $R_{\mathrm{eff}} \ll r_s$, the system is in a strongly interacting regime called the unitary limit. In this regime the interparticle spacing r_s is the only relevant scale, and the rest of the quantities are universal and system independent. The total energy of this system can be written as $E = \xi E_{\mathrm{free}}$, where E_{free} is the energy of the non-interacting atomic gas and ξ is a system independent parameter. Experimental measurements of ξ have been performed using ^{6}Li and ^{40}K atoms by investigating the expansion rate of the atomic cloud and the sound propagation in it [8–12]. Simultaneously, a number of theoretical and numerical estimations of ξ have been reported, including diffusion Monte Carlo (DMC) [13–18] as well as path integral Monte Carlo, lattice simulations and analytical methods [18–27]. The resulting estimates fall between ≈ 0.25–0.45 showing that the actual value has not been settled yet and is still of significant interest due to the universal nature of the unitary limit.

One of the most interesting properties of the unitary gas is the robust presence of the pairing condensate which involves a large fraction of the system. The study of pairing effects is thus much more straightforward than, say, in superconducting materials, where only a sliver of the fermions around the Fermi level forms the condensate and the attractive interaction is much more complicated. The quantum Monte Carlo (QMC) methods have the advantage that the condensate can be detected directly, by evaluating the off-diagonal two-particle density matrix and by monitoring its behavior at large distances [16, 18].

The goal of our study is twofold. First, the actual simulations are performed for a non-vanishing, albeit possibly very small, interaction range R_{eff}, whereas R_{eff} should not be present in any result in the unitary limit. It is necessary to analyze whether the actual limit of infinite dilution, or, equivalently, of point-like character of the interaction, has indeed been reached. Second, the impact of the fixed-node approximation in the quantum Monte Carlo method is not very well understood for this system since there is nothing to compare with: so far the fixed-node formulation of the QMC methods appears to be the only approach that is able to provide an upper bound for the total energy. This has motivated us to probe the accuracy of the nodes by released-node QMC simulations and by exploring the variational flexibility of the employed wave functions.

We have carried out calculations of the ground-state properties of a dilute Fermi gas by the fixed-node DMC (FN-DMC) [28] method for 4, 14, 38 and 66 atoms. The two-particle potential was tuned to $a_s \to \infty$. To fulfill the second condition of the unitary regime, $R_{\mathrm{eff}} \ll r_s$, the simulations were repeated for varied R_{eff} and the results were extrapolated to $R_{\mathrm{eff}} = 0$ in the end. The early calculations of the parameter ξ [13, 14] as well as some recent studies [18] were done at $R_{\mathrm{eff}}/r_s \approx 0.17$. We have found that the extrapolation from this point to zero corresponds to over 5% reduction of the ξ value consistent

with other very recent investigations [29, 30].

In order to test the quality of the nodal surface of the BCS wave function, we have performed released-node DMC (RN-DMC) [31, 32] calculations for 4 and 14 atoms. This procedure has been carried out starting from two types of nodal constraints: from the BCS nodes and from the Hartree-Fock (HF) nodes. Our RN-DMC results suggest that the nodal corrections are driven mainly by long-range correlations which are difficult to sample in the released-node framework due to the rapid growth of the bosonic noise. Nonetheless, we have been able to conclude that the fixed-node error is marginal for the BCS wave function in the case of the smallest system consisting of 4 atoms.

We have calculated also the two-body density matrix and the condensate fraction for the 66 atom system, and we have estimated the corrections from the effective-range extrapolation to these quantities.

II.   METHOD

A.   Hamiltonian

We consider a two-component Fermi gas with Hamiltonian

$$H = -\frac{1}{2} \sum_{i=1}^{N/2} \nabla_i^2 - \frac{1}{2} \sum_{i'=1}^{N/2} \nabla_{i'}^2 + \sum_{i,i'} V(r_{ii'}) , \qquad (1)$$

where N is the total number of atoms, i and i' correspond to the spin-up and spin-down atoms, and $r_{ii'}$ denotes the distance $|\mathbf{r}_i - \mathbf{r}_{i'}|$. The atoms are located in a cubic box with the side L and we impose the periodic boundary conditions. The two-particle potential $V(r_{ii'})$ is taken in the Pöschl-Teller form

$$V(r_{ii'}) = -\frac{2\mu^2}{\cosh^2(\mu r_{ii'})} , \qquad (2)$$

whose effective range is $R_{\text{eff}} = 2/\mu$. The s-wave scattering length a_s is infinite for all values of $\mu \neq 0$.

B.   Trial wave functions

In the majority of our calculations we employ trial wave functions of the BCS form multiplied with the Jastrow factor (BCS-Jastrow) as given by

$$\Psi_T(\mathbf{R}) = \Psi_{BCS}(\mathbf{R}) e^{J(\mathbf{R})} , \qquad (3)$$

where

$$\Psi_{BCS}(\mathbf{R}) = \mathcal{A} \left[\prod_{i,i'=1}^{N/2} \phi(\mathbf{r}_i, \mathbf{r}_{i'}) \right] = \det[\phi(\mathbf{r}_i, \mathbf{r}_{i'})] . \qquad (4)$$

Here $\mathcal{A}$ represents the antisymmetrization operator and $\phi(\mathbf{r}_i, \mathbf{r}_{i'})$ is the pair orbital. The vector $\mathbf{R}$ encompasses all atomic coordinates $\mathbf{r}_i$ and $\mathbf{r}_{i'}$. Additionally, we have carried out a subset of calculations also with the Hartree-Fock-Jastrow (HF-Jastrow) trial functions, in which Ψ_{BCS} is replaced with a product of two Slater determinants of one-particle orbitals (simple plane waves). The HF-Jastrow wave function reads as

$$\Psi_{SJ}(\mathbf{R}) = \det[\varphi_a(\mathbf{r}_i)] \det[\varphi_a(\mathbf{r}_{i'})] e^{J(\mathbf{R})} . \qquad (5)$$

The pair orbital $\phi(\mathbf{r}_i, \mathbf{r}_{i'})$ in Ψ_{BCS} is written as a linear combination of Gaussian functions

$$\phi(\mathbf{r}_i, \mathbf{r}_{i'}) = \sum_{l,m,n=-1}^{1} \sum_k d_k e^{-\alpha_k(x_i - x_i' + lL)^2}$$
$$\times e^{-\alpha_k(y_i - y_i' + mL)^2} e^{-\alpha_k(z_i - z_i' + nL)^2} , \qquad (6)$$

where d_k are expansion coefficients, and $\mathbf{r}_i = (x_i, y_i, z_i)$ and $\mathbf{r}_{i'} = (x_{i'}, y_{i'}, z_{i'})$ are coordinates of i and i' atoms inside the simulation box. We choose sufficiently large exponents α_k so that only the first neighbor shell of periodic images contributes to the sum, that is, the Gaussian functions are negligible at distances larger than $3L/2$. The pair orbital is smooth with zero derivative at the boundary of the simulation cell. The Jastrow factor $J(\mathbf{R})$ is constructed in a similar way as the pair orbital $\phi(\mathbf{r}_i, \mathbf{r}_{i'})$ and contains contributions for both different spin atoms and same spin atoms.

A typical trial wave function includes around 30 to 40 variational parameters that are optimized by minimizing a linear combination of the total energy and its variance [33]. Although the Jastrow factor does not change the nodal surface, accurate description of the pair correlations makes the variational optimization much more efficient and robust. When the effective range of the potential approaches zero, more Gaussian functions with larger exponents α_k are included in the Jastrow factor in order to keep the accuracy of the trial function consistently high. On the other hand, and somewhat surprisingly, we find that similar adjustment of the pair orbital with the changing effective range is relatively minor.

C.   Fixed-node and released-node DMC methods

The DMC method projects out the ground state from a given trial function Ψ_T by means of an auxiliary evolution in the imaginary time, $\Phi(\tau) \sim \exp(-\tau H)\Psi_T$. By introducing importance sampling [28] with the aid of a guiding function Ψ_G, we can write an integral equation for $\Phi(\mathbf{R}, \tau)$ in the form

$$\Psi_G(\mathbf{R})\Phi(\mathbf{R}, \tau + \Delta\tau) =$$
$$\int d\mathbf{R}' \frac{\Psi_G(\mathbf{R})}{\Psi_G(\mathbf{R}')} G(\mathbf{R}, \mathbf{R}', \Delta\tau)\Psi_G(\mathbf{R}')\Phi(\mathbf{R}', \tau) . \qquad (7)$$
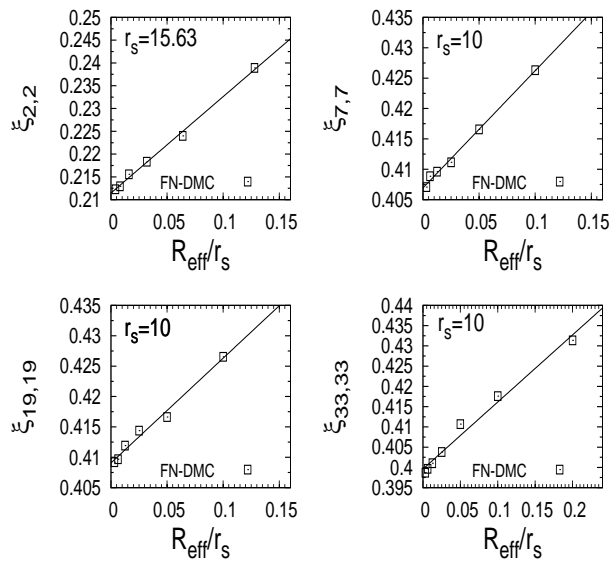
FIG. 1. The fixed-node energy for unpolarized unitary Fermi gas as a function of the interaction range R_{eff}/r_s with linear extrapolation to $R_{\text{eff}}/r_s = 0$. The system sizes are 4, 14, 38 and 66 atoms from the top left to the bottom right. The statistical error bars are smaller than the symbol size.

For small $\Delta\tau$, the propagator $G(\mathbf{R}, \mathbf{R}', \Delta\tau)$ can be approximated using the Trotter-Suzuki formula as

$$\frac{\Psi_G(\mathbf{R})}{\Psi_G(\mathbf{R}')} G(\mathbf{R}, \mathbf{R}', \Delta\tau) \approx G_0(\mathbf{R}, \mathbf{R}' + \Delta\tau \mathbf{v}(\mathbf{R}'), \Delta\tau)$$
$$\times e^{-\Delta\tau[E_L(\mathbf{R}) + E_L(\mathbf{R}') - 2E_T]/2}, \quad (8)$$

where $\mathbf{v}(\mathbf{R}') \equiv \nabla \ln |\Psi_G(\mathbf{R}')|$ and $G_0(\mathbf{R}, \mathbf{R}', \Delta\tau)$ is the Green's function for non-interacting atoms that takes the form of the diffusion kernel. The so-called local energy E_L is given by

$$E_L(\mathbf{R}) = \frac{H\Psi_G(\mathbf{R})}{\Psi_G(\mathbf{R})} \,. \quad (9)$$

The product $\Psi_G \Phi$ is represented by a set of samples (also referred to as walkers) and this ensemble is evolved with the aid of a stochastic process simulating Eqs. (7) and (8). In the fixed-node method we set $\Psi_G(\mathbf{R}) = \Psi_T(\mathbf{R})$ and the fixed-node condition is imposed by enforcing the sampling points to obey

$$\Psi_G(\mathbf{R})\Phi(\mathbf{R}, \tau) \geq 0 \quad (10)$$

at all times. In the limit of long τ the solution converges towards the lowest-energy state consistent with the boundary conditions given by the fixed nodes.

In the RN-DMC method the guiding function has bosonic symmetry and its square should be close to the square of the fermionic ground state. We have used guiding functions in the form [32, 34]

$$\Psi_G(\mathbf{R}) = \sqrt{\Psi_T^2(\mathbf{R}) + \alpha \langle \Psi_T^2 \rangle}, \quad (11)$$

where $\langle \Psi_T^2 \rangle$ is the average value of $\Psi_T^2(\mathbf{R}_0)$ over all configurations, and $\mathbf{R}_0$ are the walker positions right after the nodal release. The tunable parameter α controls the rate of walkers passing through the nodal region. The guiding function is non-negative everywhere and therefore the stochastic process propagates a mix of bosonic and fermionic states. The fermionic component is filtered out by reweighting with the factor Ψ_T/Ψ_G so that the fermionic-state energy is given by

$$\langle \Phi_0 | H | \Psi_T \rangle = \frac{\int d\mathbf{R} \Phi_0(\mathbf{R}) \Psi_G(\mathbf{R}) \frac{\Psi_T(\mathbf{R})}{\Psi_G(\mathbf{R})} \frac{H\Psi_T(\mathbf{R})}{\Psi_T(\mathbf{R})}}{\int d\mathbf{R} \Phi_0(\mathbf{R}) \Psi_G(\mathbf{R}) \frac{\Psi_T(\mathbf{R})}{\Psi_G(\mathbf{R})}} , \quad (12)$$

where $\Phi_0(\mathbf{R})$ denotes the exact fermionic ground state.

Since this method is exponentially demanding both in the projection time and in the number of atoms, it is important to choose α so that the statistical information is recovered as quickly as possible. If α is too large the fluctuations from the poor importance sampling overwhelm any useful signal very rapidly. On the other hand, a too small value can bias the results. The converged RN-DMC energy should not depend on α, provided one would be able to evolve the stochastic process with the error bars under control until the full convergence. Since it is difficult to reach reliable error bars in this type of calculations, we have used the method mostly to identify the onset and the amplitude of the energy decrease during the projection period when the stochastic noise was acceptably small.

In the RN-DMC process, we can also pick up the statistical signal from the walkers that have never crossed the nodal surface, and in essence this provides the FN-DMC estimator. By monitoring these paths as well, we can assess the consistency of the estimators and somewhat better tune the parameter α for providing better RN-DMC signal.

III. RESULTS

For benchmark purposes we first calculate perhaps the smallest nontrivial system—four atoms. Our result is shown in Fig. 1, upper left panel. There is approximately 10% energy drop when R_{eff}/r_s is reduced from 0.1279 to 0.003998. We extrapolate R_{eff} to zero using a linear fit and obtain $\xi_{2,2} = 0.212(2)$. Here and in the rest of the paper, the denominator E_{free} in the ratio $\xi = E/E_{\text{free}}$ is evaluated in the same finite volume subject to the same boundary conditions as the nominator E.

The ground-state energy of this small and relatively simple system was obtained also by two other numerical methods using a lattice formulation of the unitary Fermi gas model: the iterative Lanczos diagonalization and the auxiliary-field projection Monte Carlo method [35]. The agreement between our fixed-node DMC results and the outcome of these entirely different methods strongly suggests that our range-extrapolated total energy of the four-atom system is very accurate. This
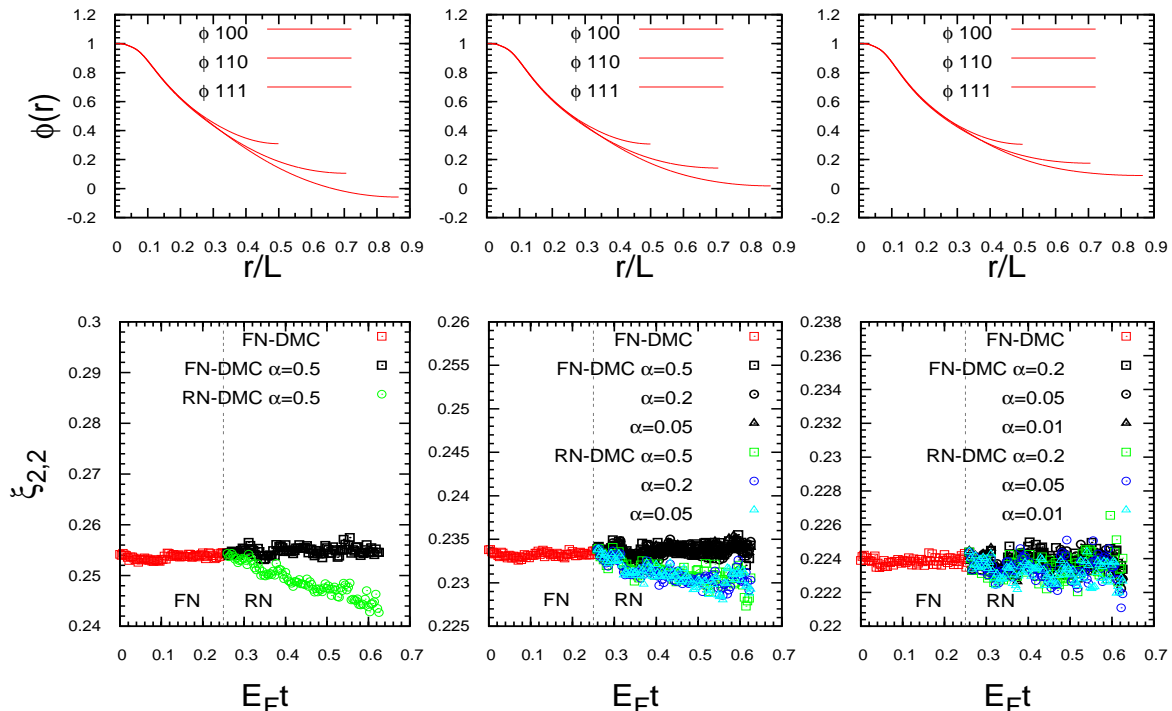
FIG. 2. (Color online) The pair orbitals and FN-DMC and RN-DMC energies of the 4-atom unitary system with $R_{\mathrm{eff}}/r_s = 0.06397$. The upper row shows the pair orbitals with the lowest (left), intermediate (middle) and optimal (right) accuracy with regard to the variational optimization. The lower row shows the corresponding DMC energies as functions of the projection time starting from the variational estimate. Note that the resolution of the left and right panels differs by an order of magnitude. The vertical dotted lines indicate the instant of the nodal release.

conclusion is further corroborated by our released-node DMC results discussed below.

Our calculations with 14, 38 and 66 atoms are carried out analogously to the 4-atom case, and the extrapolated values of ξ are 0.407(2), 0.409(3) and 0.398(3), respectively, as plotted in Fig. 1. In these calculations, the smallest effective range is $R_{\mathrm{eff}}/r_s = 0.003125$. Reduction of R_{eff} decreases the energy in all cases although the decrease per atom is smaller in larger systems.

To test the quality of the nodal surfaces, we have carried out released-node calculations for 4-atom and 14-atom systems. In a typical released-node run the number of walkers was about two million so that the error bars were initially very small. Time step $\Delta\tau$ was set to $4 \times 10^{-5} r_s^2$ in all cases and we have verified that the time-step bias of the results is negligible.

The RN-DMC calculations for 4 atoms were done with $R_{\mathrm{eff}}/r_s = 0.06397$. In Fig. 2, the upper row shows the pair orbital along three distinct directions (100, 110 and 111) of the interparticle distance vector $\mathbf{r}_i - \mathbf{r}_j$. The lower row shows the FN-DMC and RN-DMC energies as they evolve with the projection time. The plots show convergence of the FN-DMC energy followed by the nodal release. This is accomplished by switching the guiding wave function from $\Psi_T(\mathbf{R})$ to the bosonic function $\Psi_G(\mathbf{R})$ defined in Eq. (11).

The released-node signal reflects the quality of the nodal surface of the trial wave function employed in the FN-DMC simulation. We have tested wave functions with intentionally varied accuracy by employing suboptimal pair orbitals. The plot of the energy evolution in the left panel of Fig. 2 shows a clear and pronounced drop after the nodal release. As the quality of the pair orbital improves, this drop shrinks. For the fully optimized BCS-Jastrow wave function (the right panel in Fig. 2) the energy is reduced by less than 0.002 within the longest projection time we have tried. Despite the RN-DMC energies do not converge within the simulation time, it is apparent that the released-node method successfully detects the nodal inaccuracies that were intentionally introduced into the wave functions. In addition, as expected, the amplitude of the released-node signal qualitatively corresponds to the size of the introduced nodal deficiencies: the larger the nodal distortion the stronger the nodal release response. For our best wave function there is essentially no released-node signal visible within the obtained error bars and projection times. This fact as well as comparison with other two numerical methods [35] indicate that our fully optimized BCS wave functions are very accurate in this small system and that the fixed-node error is marginal.

We observe an unexpectedly high sensitivity of the
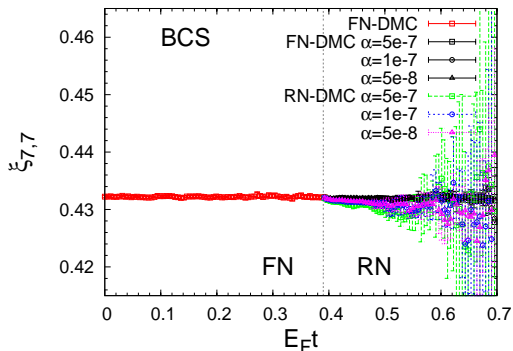
FIG. 3. (Color online) Evolution of the DMC energies for the 14-atom system with the best optimized BCS-Jastrow wave function. The runs are for $R_{\mathrm{eff}}/r_s = 0.2$. No statistically significant energy drop is observed after the nodal release that is indicated with the vertical dotted line.

FIG. 4. (Color online) DMC energies for 14 atoms obtained with the Slater-Jastrow wave function. The runs are for $R_{\mathrm{eff}}/r_s = 0.2$. The RN-DMC energy drops are significant when compared to the RN-DMC signal from the BCS-Jastrow wave function. The parameter $\xi_{7,7}$ drops by ≈ 0.015 within $E_F t \approx 0.2$ after the nodal release.

nodal quality to the details of the pair orbital at large distances. Although the suboptimal orbitals used in the 4-atom RN-DMC simulations were modified only in their long-range tails (see the upper row of Fig. 2), the fixed-node energies did raise by sizable amounts. This suggests an explanation for the relatively slow convergence of the released-node energy: the long-range tails of the pair orbital affect the nodal hypersurfaces, although the energy cost of nodal hypersurfaces displacement is surprisingly low (this has been actually tested very recently on another system, see [36]). One can further deduce that this makes the released-node method quite challenging to apply since it requires correcting the nodal surface change by sampling low-density regions with walkers travelling large distances. This is, however, difficult to achieve since the diffusive motion of walkers is slow, proportional to $t^{1/2}$, while the growth of the noise is fast, proportional to $\exp(\Delta_{BF} t)$, where Δ_{BF} is the difference between the bosonic and fermionic ground-state energies.

The RN-DMC energy for 14 atoms with $R_{\mathrm{eff}}/r_s = 0.2$ is shown in Fig. 3. The error bars are estimated from eight independent runs with two million walkers each. In the interval of $E_F t \leq 0.2$ after the nodal release the RN-DMC energy gain appears to be very small and the error bars preclude to make any statistically sound estimation for longer projection times. The rapid loss of resolution is expected since the difference between the bosonic and fermionic ground states grows with the number of atoms. Again, the RN-DMC signal exhibits little dependence on α we choose.

In order to make a comparison with a case displaying a clear fixed-node bias, we have carried out RN-DMC runs using the Slater-Jastrow trial wave function, see Fig. 4. Since this wave function has the nodal surface of the noninteracting Fermi gas, the nodal surface is strongly distorted. As a result, we see a pronounced released-node signal. However, within the projection time interval of
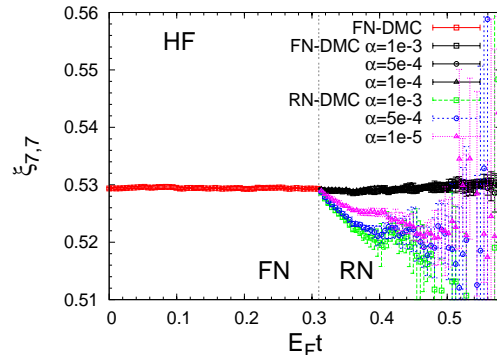
$E_F t \leq 0.2$, the energy drops by only ≈ 0.015 for the largest α we tested. This is very small considering that the true ground-state energy is at least an order of magnitude lower, which illustrates the challenges of efficient application of the released-node method, at least for the present cases. Nevertheless, the released-node method clearly detects the existence of the nodal errors associated with the Slater wave function. Although we cannot make a definite assessment of the fixed-node errors of our BCS wave functions, the comparison of Figs. 3 and 4 indicates that they are considerably smaller than the fixed-node errors of the Slater determinant.

In order to quantify the pairing effects we calculate the two-body density matrix which enables us to evaluate the condensate fraction. The projected two-body density matrix for spin-up and spin-down atoms is defined as

$$\rho^{(2)}(\mathbf{r}) = \frac{N^2}{4V^2} \frac{\int d\mathbf{R}\, \Phi(\mathbf{R})\Psi_T(\mathbf{R})\frac{\Psi_T(\mathbf{r}_1+\mathbf{r},\mathbf{r}_2+\mathbf{r})}{\Psi_T(\mathbf{r}_1,\mathbf{r}_2)}}{\int d\mathbf{R}\, \Phi(\mathbf{R})\Psi_T(\mathbf{R})}, \quad (13)$$

where N is the total number of atoms and V is the volume of the simulation cell. The density matrices have been calculated for the fixed-node wave functions and hence they correspond to the mixed estimators [28]. Nevertheless, the mixed-estimator bias is negligible since the variational Monte Carlo and DMC estimates of $\rho^{(2)}$ coincide within error bars. This is a further evidence of the high accuracy of our trial wave functions.

The condensate fraction can be extracted from the two-body density matrix as

$$c = \frac{2V^2}{N} \lim_{r\to\infty} \rho^{(2)}(r). \quad (14)$$

The calculated density matrices are shown in Fig. 5 with the condensate fraction estimated from the long-range limit. The condensate fraction saturates for $R_{\mathrm{eff}} \leq 0.5$
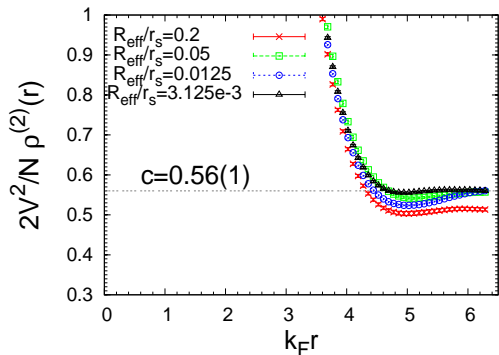
FIG. 5. (Color online) The two-body density matrix for 66 atoms calculated from the FN-DMC mixed estimator. The condensate fraction converges to 0.56(1) for $R_{\rm eff}/r_s \leq 0.05$.
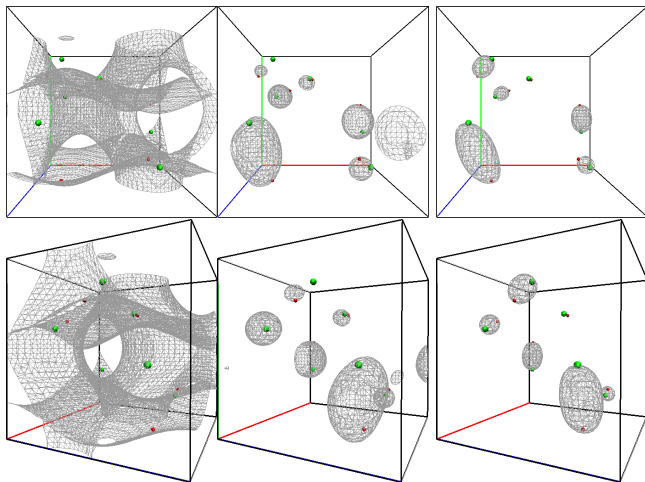
FIG. 6. (Color online) Three-dimensional subsets of the nodal hypersurfaces for three types of wave functions and corresponding phases in the 14-atom system. The node is obtained by scanning the simulation cell with a pair of spin-up and spin-down atoms sitting on the top of each other while keeping the rest of the atoms at fixed positions (tiny spheres). From the left to the right, the columns show the nodal surfaces of the wave functions corresponding to the free Fermi gas, the unitary limit and the BEC side of the crossover. The lower row displays the same surfaces rotated by 45 degrees around the z-axis.

at $c = 0.56(1)$. This value is not too far from the results obtained previously [16, 18].

To illustrate the character of the nodal surfaces in the BCS-BEC systems, we present three-dimensional scans of the nodes for three wave functions corresponding to the following scattering regimes: the free atomic gas with no pairing, our best unitary-limit wave function, and the wave function with enhanced pairing from the BEC side of the BEC-BCS phase diagram ($a_s k_F = 0.6592$). The left column of Fig. 6 displays the nodal surface of the free atomic Fermi gas. The delocalized nature of the system is apparent. At the unitary limit, shown in the middle column of Fig. 6, the shape of the nodal surface is significantly different as the pairing effects clearly dominate and lead to a localized character of the nodes from the perspective of a pair of up and down spin atoms. The nodes on the BEC side (the right column) do not differ much from the unitary limit, except for a slightly more pronounced localization.

IV. CONCLUSIONS

We have carried out QMC calculations of the zero-temperature, spin-unpolarized atomic Fermi gas in the unitary limit. We show that non-vanishing interaction range $R_{\rm eff}$ impacts the resulting total energies significantly while our data for finite $R_{\rm eff}$ agree with comparable results found in the literature. By extrapolating $R_{\rm eff}$ to zero we obtain the ratio $E/E_{\rm free}$ for 4, 14, 38 and 66 atoms to be 0.212(2), 0.407(2), 0.409(3) and 0.398(3). These extrapolated results are $\approx 5\%$ lower than the previous DMC calculation with similar quality of trial wave functions [13, 14, 18], illustrating thus the importance of extrapolation of $R_{\rm eff}$ to zero for reaching the unitary limit of the dilute atomic gas.

A similar study where an interaction-range extrapolation was also performed was very recently published in [29, 30]. The final result for the 66-atom system was $\xi_{33,33} = 0.383(2)$, which is approximately 4% lower than ours. We believe that a large portion of the difference can be attributed to differences in the functional forms of the pair orbital. Some influence could also possibly come from the differences between the extrapolation methods employed in this work and in Ref. [30].

We have performed the released-node DMC calculations for 4 and 14 atoms with different types of wave functions with intentionally varied nodes. Our release-node results for 4 atoms indicate that fully optimized BCS wave function is very accurate and the fixed-node error is marginal for this small system. For larger system of 14 atoms, we have found that the convergence to the correct and asymptotically exact ground-state energies is unfavorably slow compared to the growth of the statistical noise. We were able to identify only small energy gains within the simulation times that allowed for acceptable signal to noise ratio. Despite that, our calculations have shed new light on the remaining nodal errors which are related to the less accurate description of the low-probability regions of the configuration space. As the concurrently obtained results [30] suggest, further improvements of the BCS wave function nodes are probably not completely exhausted yet.

In addition to calculations of energies, we have evaluated the two-body density matrix and the condensate fraction in the limit of zero interaction range, and we have found only small changes in these quantities when compared with the previous calculations. Our condensate fraction from the fixed-node DMC simulations is 0.56(1).

ACKNOWLEDGMENTS

[1] W. Ketterle, Rev. Mod. Phys. **74**, 1131 (2002).
[2] W. Ketterle and M. W. Zwierlein, arXiv:0801.2500v1 (2008).
[3] S. Giorgini, L. P. Pitaevskii, and S. Stringari, Rev. Mod. Phys. **80**, 1215 (2008).
[4] U. Fano, Phys. Rev. **124**, 1866 (1961).
[5] H. Feshbach, Ann. Phys. (NY) **19**, 287 (1962).
[6] S. Inouye, M. R. Andrews, J. Stenger, H. J. Miesner, D. M. Stamper-Kurn, and W. Ketterle, Nature **392**, 151 (1998).
[7] P. Courteille, R. S. Freeland, D. J. Heinzen, F. A. van Abeelen, and B. J. Verhaar, Phys. Rev. Lett. **81**, 69 (1998).
[8] M. Bartenstein, A. Altmeyer, S. Riedl, S. Jochim, C. Chin, J. H. Denschlag, and R. Grimm, Phys. Rev. Lett. **92**, 120401 (2004).
[9] T. Bourdel, L. Khaykovich, J. Cubizolles, J. Zhang, F. Chevy, M. Teichmann, L. Tarruell, S. J. J. M. F. Kokkelmans, and C. Salomon, Phys. Rev. Lett. **93**, 050401 (2004).
[10] J. Kinast, A. Turlapov, J. E. Thomas, Q. Chen, J. Stajic, and K. Levin, Science **307**, 1296 (2005).
[11] J. T. Stewart, J. P. Gaebler, C. A. Regal, and D. S. Jin, Phys. Rev. Lett. **97**, 220406 (2006).
[12] J. Joseph, B. Clancy, L. Luo, J. Kinast, A. Turlapov, and J. E. Thomas, Phys. Rev. Lett. **98**, 170401 (2007).
[13] J. Carlson, S. Y. Chang, V. R. Pandharipande, and K. E. Schmidt, Phys. Rev. Lett. **91**, 050401 (2003).
[14] S. Y. Chang, V. R. Pandharipande, J. Carlson, and K. E. Schmidt, Phys. Rev. A **70**, 043602 (2004).
[15] G. E. Astrakharchik, J. Boronat, J. Casulleras, and S. Giorgini, Phys. Rev. Lett. **93**, 200404 (2004).
[16] G. E. Astrakharchik, J. Boronat, J. Casulleras, and S. Giorgini, Phys. Rev. Lett. **95**, 230405 (2005).
[17] S. Y. Chang and V. R. Pandharipande, Phys. Rev. Lett. **95**, 080402 (2005).
[18] A. J. Morris, P. López Ríos, and R. J. Needs, Phys. Rev. A **81**, 033619 (2010).
[19] D. Lee, Phys. Rev. B **73**, 115112 (2006).
[20] D. Lee, Phys. Rev. C **78**, 024001 (2008).
[21] V. K. Akkineni, D. M. Ceperley, and N. Trivedi, Phys. Rev. B **76**, 165116 (2007).
[22] E. Burovski, N. Prokof'ev, B. Svistunov, and M. Troyer, Phys. Rev. Lett. **96**, 160402 (2006).
[23] V. Gurarie and L. Radzihovsky, Ann. Phys. **322**, 2 (2007).
[24] A. Bulgac, J. E. Drut, and P. Magierski, Phys. Rev. Lett. **96**, 090404 (2006).
[25] A. Bulgac, J. E. Drut, and P. Magierski, Phys. Rev. A **78**, 023625 (2008).
[26] T. Abe and R. Seki, Phys. Rev. C **79**, 054002 (2009).
[27] T. Abe and R. Seki, Phys. Rev. C **79**, 054003 (2009).
[28] W. Foulkes, L. Mitas, R. J. Needs, and G. Rajagopal, Rev. Mod. Phys. **73**, 33 (2001).
[29] M. M. Forbes, S. Gandolfi, and A. Gezerlis, Phys. Rev. Lett. **106**, 235303 (2011).
[30] S. Gandolfi, K. E. Schmidt, and J. Carlson, Phys. Rev. A **83**, 041601 (2011).
[31] D. M. Ceperley and B. J. Alder, Phys. Rev. Lett. **45**, 566 (1980).
[32] D. M. Ceperley and B. J. Alder, J. Chem. Phys. **81**, 5833 (1984).
[33] C. J. Umrigar and C. Filippi, Phys. Rev. Lett. **94**, 150201 (2005).
[34] J. Casulleras and J. Boronat, Phys. Rev. Lett. **84**, 3121 (2000).
[35] S. Bour, X. Li, D. Lee, U.-G. Meißner, and L. Mitas, Phys. Rev. A **83**, 063619 (2011).
[36] K. Rasch and L. Mitas, to appear on arXiv..